# The Broad-Line Region in Active Galactic Nuclei

B.M. Peterson

Department of Astronomy, The Ohio State University, 140 West 18th Avenue, Columbus, OH 43210, USA
peterson@astronomy.ohio-state.edu

**Abstract.** We review the basic observed and inferred properties of the broad emission-line region in AGNs, as well as the basics of the reverberation-mapping technique that can be used to determine the size and structure of the region. We argue that the current best evidence points to a multi-component line-emitting region, with a disk-like structure, possibly an extension of the accretion disk itself, and a disk wind being strong candidates for the origin of the broad-line emission.

## 1 Introduction

Some 40 years after the discovery of quasars and 60 years after the publication of C.K. Seyfert's initial observations of high central surface brightness galaxies, we are finally quite certain that active galactic nuclei (AGNs) are powered by accretion onto supermassive collapsed objects. While many important details remain poorly understood, the black-hole/accretion-disk paradigm is now reasonably secure. In contrast, however, we still have no self-consistent models of the nuclear regions that produce (a) the broad emission lines that are so prominent in the UV/optical spectra of AGNs and (b) the strong absorption features seen in the X-ray/UV spectra. Given the proximity of these regions to the central engine, it seems likely that these are some manifestation of the accretion process and related outflow; there is a good deal of empirical evidence that connects these spectral features to disk-related outflows. Unfortunately, solid information about the broad-line region (BLR) is hard to come by: the BLR is spatially unresolved in even the nearest AGNs and the information in line profiles, sampling only one of six dimensions in phase space, is highly ambiguous.

In this review, we will concentrate on a few things that we can infer about the nature of the BLR, and reverberation mapping, arguably the most promising technique for exploring the nature of the BLR. The scope of this review is limited to a few basic topics and represents, of course, the author's own highly biased personal view.

B.M. Peterson: *The Broad-Line Region in Active Galactic Nuclei*, Lect. Notes Phys. **693**, 77–100 (2006)
DOI 10.1007/3-540-34621-X_3 

## 2 Basic Inferences about the Line-Emitting Gas

The relative strengths of the various emission lines in AGN spectra are very similar to those emitted by a wide variety of astrophysical plasmas: to some low order of approximation, the emission lines of planetary nebulae, H II regions, supernova remnants, and AGN emission-line regions are all quite similar. The reason is simple: photoionization equilibrium of all these gases is achieved at the same temperature, $T \approx 10^4$ K, e.g., [20, 21, 23, 28].

Photoionization equilibrium is attained when the rate of photoionization is balanced by the rate of recombination. The conditions where this occurs can be expressed in terms of an "ionization parameter"

$$U = \frac{Q_{\rm ion}({\rm H})}{4\pi r^2 c n_e} \ , \tag{1}$$

where $Q_{\rm ion}({\rm H})$ is the number of H-ionizing photons produced per second by the central source, i.e.,

$$Q_{\rm ion}({\rm H}) = \int \frac{L_\nu}{h\nu}\, d\nu \ , \tag{2}$$

and the integral is over ionizing photon energies and $L_\nu$ is the specific luminosity of the ionizing source. The ionization parameter is thus the ratio of the density of ionizing photons $Q_{\rm ion}/4\pi r^2 c$, reflecting ionization rate, divided by the electron density $n_e$, reflecting recombination rate, at the face of a cloud exposed to the radiation. Over a rather broad range in $U$, photoionization equilibrium is realized at electron temperatures in the range 10,000 to 20,000 K. As a result, the line spectra emitted by such gases are very similar, since variations in elemental abundances are also relatively minor. There are, of course, more subtle spectral differences among these various $10^4$ K gases which are attributable to differences in gas density $n_e$, the input ionizing spectrum, the gas dynamics, and elemental abundances (which appear to be approximately solar or slightly enhanced in AGN emission-line regions) [14].

Since at least the work of Khachikian and Weedman in the mid-1970s, it has been recognized that AGN emission-line spectra are kinematically composite. The "narrow components" have Doppler widths usually less than around 500 km s$^{-1}$; these emission lines arise in relatively low-density ($n_e \approx 10^3$ cm$^{-3}$) gas that is spatially extended – indeed, the narrow-line region (NLR) is at least partially resolved in some of the nearest AGNs. In contrast, the "broad components" have Doppler widths in the range ∼1000 to 25,000 km s$^{-1}$ and arise in gas of fairly high density by nebular standards (i.e., $n_e > 10^9$ cm$^{-3}$), as determined from the weakness of certain metastable and forbidden lines that are relatively more prominent in lower-density gases.

Indeed, the gas density leads us to an important distinction that is not obvious based on line widths alone: the widest narrow lines and the narrowest broad lines have similar Doppler widths, around 1000 km $^{-1}$ (though not in the same object: in general, there is a correlation between the widths of the

narrow and broad lines in AGN spectra). However, even the subclass of broad-line objects known as narrow-line Seyfert 1 (NLS1) galaxies still have distinct "broader" and "narrower" features, with the difference between them being the absence of the "broader" component in the forbidden or semiforbidden lines, i.e., from the high-density gas in which these transitions are collisionally suppressed.

Temperatures of order $10^4\,\mathrm{K}$ correspond to thermal line widths of order $10\,\mathrm{km\,s^{-1}}$, so it is clear that in both the NLR and the BLR, the gas moves supersonically. This in turn suggests some kind of organized flow, or a system of discrete "clouds." The especially large Doppler widths of the broad lines immediately suggest that they may arise in a deep gravitational potential, which makes the broad lines especially valuable as probes of the central source.

Compared to the NLR, the actual amount of emission-line gas required to produce the broad emission lines can be quite modest as line emission is very efficient in high-density gases (the emissivity per unit volume is proportional to $n_e^2$). We also observe that the emission-line fluxes vary with the continuum flux, but with a short time delay. From this we infer that the broad-line emitting gas is photoionized and optically thick to ionizing continuum radiation. Moreover, we conclude that the BLR must be fairly small from light-travel time arguments. Conversely, the narrow lines do *not* vary on short time scales; the region is spatially extended, geometrically diluting the variable continuum signal over a large volume, and the recombination timescale is very long, further smearing out any temporal variations.

The kinematics of the line-emitting gas remains problematic. In the case of the NLR, the narrow-emission line widths are correlated with the stellar bulge velocity dispersions, albeit with considerable scatter in the correlation. Nevertheless, this suggests that gravitation provides an important component. However, there is also considerable evidence for interaction between the narrow lines and radio-emitting plasma that is being ejected from the nucleus.

How the BLR gas is moving, whether in infall, outflow, or orbital motion, remains unknown. Emission-line profiles alone only weakly constrain the possibilities because there are a wide variety of profoundly different kinematic models that yield similar line profiles. Broad-line profiles are distinctly non-Gaussian, and have sometimes been described as "logarithmic," i.e., the flux at some displacement $\Delta\lambda$ from line center is proportional to $-\ln\Delta\lambda$, for $\Delta\lambda$ not too close to line center. In many cases, however, the line profiles have some structure, variously described as "bumps" or "humps" or, in other cases as "asymmetric wings" or "shelves." Such features can be either prominent or subtle, and they can change over long time scales. Indeed, the persistence of features in profiles over longer than dynamical time scales $\tau_{\mathrm{dyn}} \approx R/\Delta V$, where $R$ is the size of the region and $\Delta V$ represents a typical velocity, strongly suggests that the BLR has some kind of regular structure

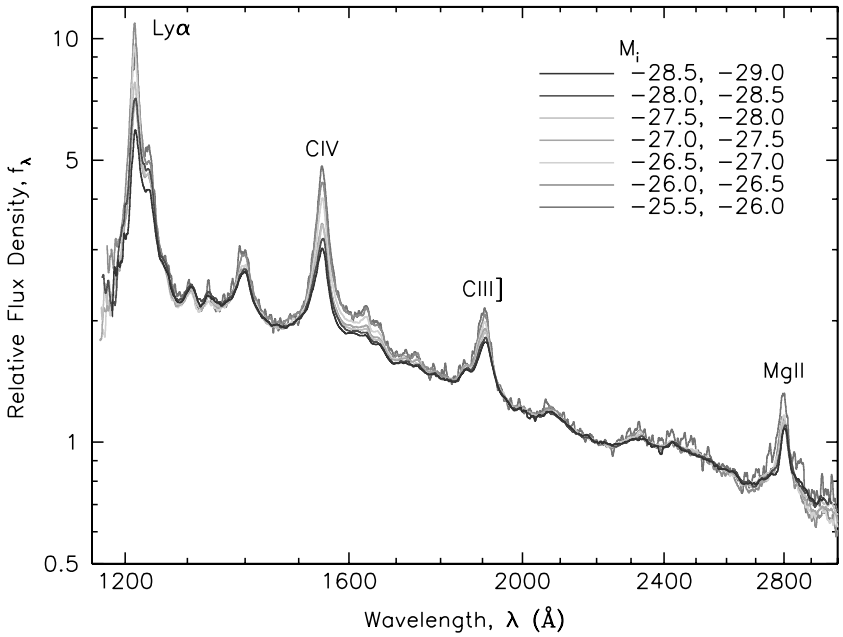


**Fig. 1.** Composite spectra from the Sloan Digital Sky Survey, binned by luminosity ($M_i$). Note the similarity of the spectra, with the exception of the "Baldwin Effect" in C IV $\lambda$1549; i.e., relative to the continuum and the other lines, C IV is stronger in lower-luminosity objects. From Vanden Berk et al., 2004, in "AGN Physics with the Sloan Digital Sky Survey" ed. G.T. Richards and P.B. Hall (San Francisco: Astronomical Society of the Pacific)

or symmetry, though variability studies, as discussed below, show that the gas is not in simple spherical outflow (like a supernovae explosion) or infall (i.e., Bondi accretion).

The average line spectra of AGNs are very similar over a wide range of luminosity, as shown in Fig. 1. This suggests that in addition to temperature, particle densities and ionization parameters are quite similar. An important exception to this statement is the behavior of the C IV $\lambda$1549 emission line; relative to the continuum, C IV is weaker in more luminous objects (i.e., its equivalent width decreases with luminosity), a well-known anticorrelation known as the Baldwin Effect. There are other obvious differences among AGNs, and many of the more subtle differences are correlated with one another; these correlated properties stand out prominently in "principal component analysis." The strongest set of correlations, known as "Eigenvector 1," reveals that strong optical Fe II emission is negatively correlated with the width of the H$\beta$ broad component and the strength of the narrow [O III] $\lambda$5007 line, e.g., [5]. It has been speculated by many investigators that Eigenvector 1 measures the Eddington ratio $\dot{M}/\dot{M}_{\rm Edd}$, i.e., the accretion rate

relative to the rate required to produce the Eddington luminosity; in terms of the observables, this is essentially the luminosity to mass ratio.

## 3 Broad Emission-Line Variability and Theory of Reverberation Mapping

As noted above, the broad emission-line fluxes are observed to vary in response to continuum variations, with a short (usually days to weeks for typical Seyfert 1 galaxies) time delay that is attributable to the light travel time across the BLR, i.e., $\tau_{\rm lt} = R/c$. This affords a potentially powerful tool; by closely examining the velocity-resolved response of the broad lines to continuum variations, the kinematics and geometry of the BLR can be determined, or at least highly constrained. Moreover, while the observations have to be done with great attention to quality and homogeneity, they are not otherwise a serious observational challenge since they involve prominent emission lines in the UV/optical spectra of relatively bright AGNs.

### 3.1 Basic Assumptions

The reverberation method as it is currently applied to AGNs rests on some simple assumptions, e.g., [4, 22, 24], which to some extent can be justified *ex post facto*:

1. *The continuum originates in a single central source.* The continuum source in typical Seyfert galaxies ($10^{13}$ – $10^{14}$ cm) is much smaller than the BLR, which reverberation reveals to be $\sim 10^{16}$ cm in these objects. Note in particular that it is not necessary to assume that the radiation from the central source is emitted isotropically.
2. *The light travel time across the BLR is the most important time scale.* Specifically, we assume that that cloud response time is instantaneous, which is a good assumption given the high densities of the BLR gas. The response time is given by the recombination time scale $\tau_{\rm rec} = (n_e \alpha_{\rm B})^{-1} \approx 0.1 (10^{10}\,{\rm cm}^{-3}/n_e)$ hours, where $\alpha_{\rm B}$ is the hydrogen case B recombination coefficient and $n_e$ is the particle density. It is also assumed that the BLR structure is stable over the duration of the reverberation experiment, which is typically no longer than several months for Seyfert galaxies, but can be much longer for high-luminosity quasars. For typical low-luminosity reverberation-mapped AGNs (i.e., Seyfert galaxies), $\tau_{\rm dyn} \approx 3$–5 years.
3. *There is a simple, though not necessarily linear, relationship between the observed continuum and the ionizing continuum.* The key element is that the ionizing continuum and observable (either satellite UV or optical) continuum vary in phase. In only two well-studied cases, NGC 7469 and Akn 564, has this assumption been critically tested. In both cases, time lags between the continuum variations at the shortest UV wavelengths

and those at the longest optical wavelengths are of order ∼1 day. In terms of amplitude of variation, the variations in the UV are generally much stronger, even after taking dilution of the optical continuum into account.

Under these simple assumptions, a simple linearized model to describe the emission-line light curve as a function of line-of-sight (LOS) velocity $V$ can be written as

$$\Delta L(t,V) = \int_0^\infty \Psi(\tau,V)\,\Delta C(t-\tau)\,d\tau\ , \tag{3}$$

where $\Delta C(t)$ and $\Delta L(t,V)$ are the differences from the mean continuum and mean LOS velocity-resolved emission-line light curves, respectively, $\tau$ is the time delay, and $\Psi(\tau,V)$ is the "transfer function" or, more descriptively, the "velocity-delay map." The velocity-delay map is thus the response of an emission line to an instantaneous or $\delta$-function continuum outburst at some time $t_0$, i.e., $C(t) = \delta(t-t_0)$. The goal of reverberation mapping is to recover the velocity-delay map from the observables, $\Delta C(t)$ and $\Delta L(t,V)$, and thus infer the structure and geometry of the line-emitting region. This represents a classical inversion problem in physics, and solution by Fourier methods immediately suggests itself. However, solution by Fourier transforms is successful only in the case of large amounts of data and low noise, neither condition which can be easily realized in astronomical observations of faint sources. A less ambitious goal is to determine the "delay map" $\Psi(\tau) = \int \Psi(\tau,V)\,dV$ by using the integrated emission-line light curve. In practice, unambiguous determination of delay maps has also been illusive. In most cases, we have to settle for an estimate of the mean time scale for response, which we obtain by cross-correlating the continuum and emission-line light curves; the mean delay time, or "lag," is usually a good estimate of the centroid of the delay map.

### 3.2 Isodelay Surfaces

As noted above, the velocity-delay map represents the response of the BLR to a $\delta$-function outburst, as seen by a distant observer. At the moment the observer detects the outburst, he will also detect the response of the emission-line gas along his line of sight to the continuum source; the total path followed by the ionizing photons that leave the central source and are replaced by emission-line photons when they encounter the BLR gas is the same path followed by the unabsorbed photons that are eventually detected by the observer. There is thus no time delay for the response of gas along the line of sight to the continuum source. For all other points, however, there will be a time delay $\tau$ between detection of the continuum outburst and the line response because of the increased path length.

Suppose for simplicity that the BLR clouds are all in a circular Keplerian orbit of radius $r$ around the central black-hole/accretion-disk structure. At

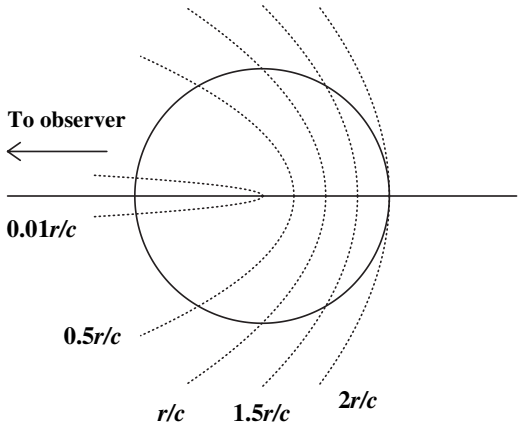


**Fig. 2.** For illustrative purposes, BLR clouds are supposed to be on circular Keplerian orbits of radius $r$ and the continuum source is a point at the center of the ring. Following a continuum outburst, at any given time the observer far to the left sees the response of clouds along a surface of constant time delay, or isodelay surface. Here we show five isodelay surfaces, each one labeled with the time delay (in units of the shell radius $r$) we would observe relative to the continuum source. Points along the line of sight to the observer are seen to respond with zero time delay. The farthest point on the shell responds with a time delay $2r/c$

any given delay $\tau$ we observe the response of all points on a surface of constant delay, or "isodelay surface," which must be a paraboloid of revolution around the line of sight. This is illustrated in Fig. 2. which shows that, compared to the signal from the central source, the signal from anywhere else on the ring is delayed by light-travel time effects.

In the upper panel of Fig. 3, we define a system of polar coordinates measured from our line of sight to the continuum source. For clouds at position $(r, \theta)$, we see that the observer detects a time delay

$$\tau = (1 + \cos\theta)r/c. \tag{4}$$

Thus, at any time delay $\tau$ relative to the detection of the outburst, the distant observer sees the response of all gas clouds that intersect with the isodelay surface defined by (4).

### 3.3 Velocity-Delay Maps

We are now prepared to construct a simple velocity-delay map from first principles. We adopt as a toy model the edge-on (inclination $i = 90°$) ring system shown in the upper panel of Fig. 3 and consider now how the points on the ring translate from $(r, \theta)$ measured in configuration space to $(V, \tau)$ measured in velocity-delay space. This is illustrated in the lower panel of

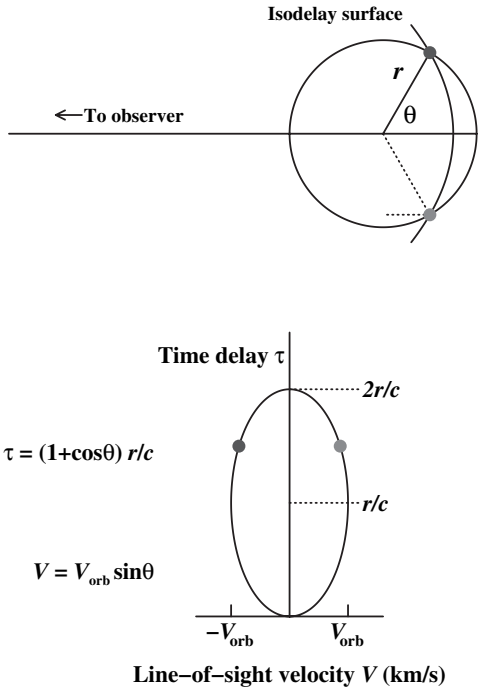


**Fig. 3.** The upper diagram shows a ring-like BLR with the observer to the left. The upper diagram shows a ring (or cross-section of a thin shell) that contains line-emitting clouds, as in Fig. 2. An isodelay surface for an arbitrary time is given; the intersection of this surface and the ring shows the clouds that are observed to be responding at this particular time. The *dotted line* shows the additional light-travel time, relative to light from the continuum source, that signals reprocessed by the cloud into emission-line photons will incur (4). In the lower diagram, we project the ring of clouds onto the LOS velocity/time-delay $(V, \tau)$ plane, assuming that the emission-line clouds in the upper diagram are orbiting in a clockwise direction (so that the cloud upper part of the orbit in the upper diagram is blueshifted and is represented on the left side of the lower diagram)

Fig. 3, where we have identified two of the emission-line clouds that lie on a particular isodelay surface. These points obviously project to $\tau = (1 + \cos\theta)r/c$ and LOS velocities $V = V_{\rm orb} \sin\theta$, where $V_{\rm orb}$ is the circular orbit speed. It is thus easy to see that an edge-on ring in configuration space projects to an ellipse in velocity-delay space, with semi-axes $V_{\rm orb}$ and $r/c$. It is also trivial to see that decreasing the inclination of the ring from 90° will decrease both axes by a factor of $\sin i$; as $i$ approaches 0, the velocity-delay ellipse contracts towards a single point at $V = 0$ (since the orbital motion is now in the plane of the sky) and $\tau = r/c$ (since all points on the ring are now equidistant from the observer).

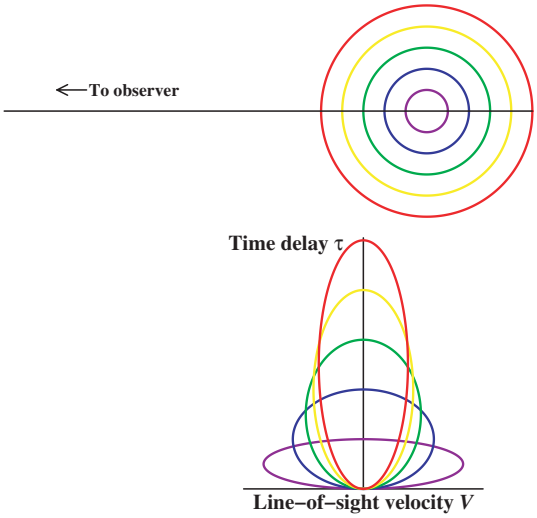


**Fig. 4.** Same information as in Fig. 3, except that here, the response is given for a multiple-ring system for clouds in circular Keplerian orbits. Each orbit projects to an ellipse in velocity–delay space. Larger orbits project to larger ranges in time delay ($2r/c$) and smaller LOS velocities ($V \propto r^{-1/2}$)

Once we have a velocity-delay map for a ring at arbitrary inclination, it is simple to take the next step to a Keplerian disk, which is essentially a sequence of rings with orbital velocities decreasing like $V_{\rm orb} \propto r^{-1/2}$. Such a sequence of rings is shown in Fig. 4.

Generalization to a disk (a series of rings), a thin shell (a series of rings of fixed $r$ and varying $i$), or a thick shell (a series of thin shells of varying $r$) is trivial because of the linear nature of (3). All simple geometries dominated by Keplerian motion will show in the velocity-delay map the same characteristic "taper" with increasing time delay as seen in Fig. 4.

The ultimate goal of reverberation mapping is to recover the velocity-delay map from the observations. Unfortunately, in no case to date has this been possible, though in fairness it must be noted that recovery of a velocity-delay map has not been the principal goal of any experiment that has been carried out as designed; virtually all previous reverberation mapping programs have been designed to measure only the mean response time of emission lines to continuum variations. Even this comparatively modest goal has led to a number of important results, as described below.

# 4 Reverberation Results

## 4.1 Size of the BLR and Scaling with Luminosity

Emission-line time delays, or lags, have been measured for 35 AGNs, in some cases for multiple emission lines. The highest ionization emission lines are found to respond most rapidly to continuum variations, demonstrating clearly that there is ionization stratification within the BLR. Moreover, the highest ionization lines tend to be *broader* than the lower ionization lines, and indeed a plot of line width versus time delay shows that the lag $\tau$ varies with line width $\Delta V$ as $\tau \propto \Delta V^{-2}$, the virial relationship expected if the dynamics of the BLR is dominated by the gravitational potential of the central source. We show the results for the well-studied case of NGC 5548 in Fig. 5, [26].

As noted earlier, AGN spectra are remarkably similar over a broad range of luminosity. We might thus infer that, to some low order of approximation, their BLRs have similar physical conditions. Specifically, referring back to (1) and (2), we might conclude that $U$ and $n_e$ are about the same in all AGNs, and from that we could easily reach the conclusion that there should be a very simple relationship between the size of the BLR and the AGN continuum luminosity [16], (since $L \propto Q$) of the simple form

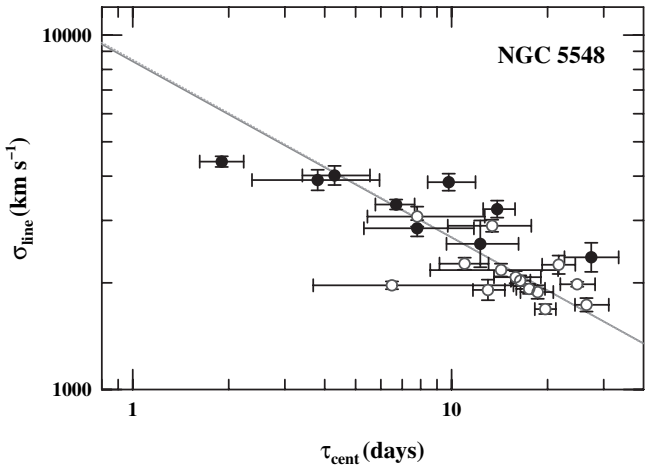


**Fig. 5.** Line width, as characterized by the line dispersion (second moment of the profile), versus time delay, as measured by the cross-correlation function centroid $\tau_{\rm cent}$, for multiple lines and multiple epochs for NGC 5548. The line measurements are for the variable part of the line only, as isolated by forming a root-mean-square (rms) spectrum from the many spectra obtained in the variability monitoring program. The *solid line* is the best fit to the data, and the *dotted line* is a forced fit to slope $-1/2$, the virial slope; in this particular case, the two lines are indistinguishable. The *open circles* are measurements of H$\beta$ for 14 different years. The *filled circles* represent all of the other lines. From [25]

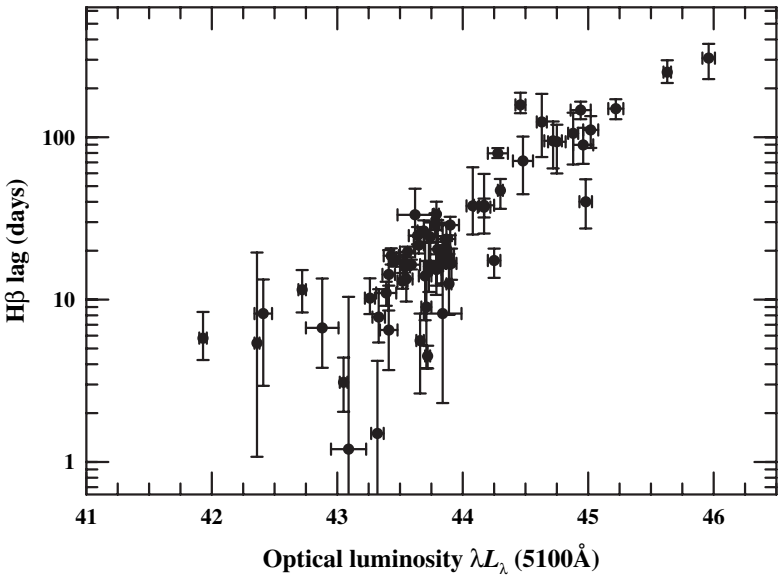


**Fig. 6.** Measured time delays for H$\beta$ versus optical luminosity for over 30 reverberation-mapped AGNs, including multiple measurements of some sources. The relationship between BLR size and luminosity can be fitted with $r(\mathrm{H}\beta) \propto L^{0.6\pm0.1}$. Based on data from [25]

$$r \propto L^{1/2} \,. \tag{5}$$

In Fig. 6, we plot the size of the broad H$\beta$-emitting region as a function of the optical luminosity at 5100 Å for over 30 AGNs, some represented by multiple measurements at different epochs. The observed slope of this correlation, $\tau(\mathrm{H}\beta) \propto L^{0.6\pm0.1}$ is surprisingly consistent with the very naive prediction of (5) over four orders of magnitude in luminosity and time delays ranging from a few days to hundreds of days.

In the case of the particularly well-observed Seyfert 1 galaxy NGC 5548, the H$\beta$ response time has been measured for 14 individual observing seasons, yielding measured lags ranging from as short as 6 days to as long as 26 days, depending on the mean continuum luminosity. The relationship between H$\beta$ lag and continuum luminosity is shown in Fig. 7. The best-fit slope to this correlation is $\tau(\mathrm{H}\beta) \propto L^{0.9}$, significantly steeper than the result obtained by comparing different objects. The explanation for this, however, seems to be simple: the shape of the continuum changes as AGNs vary. As the continuum source gets brighter, it also gets *harder*, i.e., the amplitude of variability is larger at shorter wavelengths. Comparison of the ultraviolet (1350 Å) and optical (5100 Å) continuum fluxes in NGC 5548 shows that $L_{\mathrm{opt}} \propto L_{\mathrm{UV}}^{0.56}$, and since the size of the line-emitting region is controlled by the H-ionizing continuum ($\lambda < 912$ Å), the UV flux should be a much better measure of the

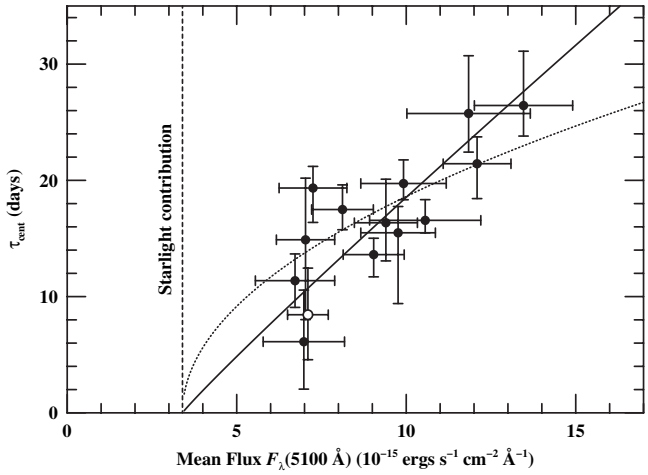


**Fig. 7.** Measured time delays for H$\beta$ in NGC 5548 versus optical continuum flux for 14 independent experiments. The vertical line shows the constant stellar contribution to the measured continuum flux. The best-fit slope to this relationship is shown as a solid line $\tau(\mathrm{H}\beta) \propto F_\lambda^{0.9}$ and the dotted line shows the naive prediction $\tau(\mathrm{H}\beta) \propto F_\lambda^{1/2}$. From [27]

ionizing flux than the optical flux. Thus, we find that

$$\tau(\mathrm{H}\beta) \propto L_{\mathrm{opt}}^{0.9} \propto (L_{\mathrm{UV}}^{0.56})^{0.9} \propto L_{\mathrm{UV}}^{0.5} \ , \tag{6}$$

again, consistent with the naive prediction.

These results lead us immediately to some uncomfortable questions. What fine-tunes the size of the BLR? How does the BLR know precisely where to be? Why are the ionization parameter and electron density the same for all AGNs?

At least a partial answer is provided by considering the result shown in Fig. 7. What is obvious from this diagram is that the H$\beta$-emitting gas of the BLR is *not* changing its location from year to year as the continuum changes; it is obviously not moving fast enough to do this. What we are forced to conclude is that gas is *everywhere* in the line-emitting region (in this case, at least between $\sim$6 and $\sim$26 light days of the central source) and that what is actually changing with time, or more properly with luminosity, is the distance from the continuum source at which the physical conditions are optimal for emission in the H$\beta$ line. This is often referred to as the "locally optimally-emitting cloud (LOC)" model, e.g., [3]. The basic idea is that line-emitting clouds of gas of various density are distributed throughout the nuclear region. Emission in a particular line comes predominantly from clouds with optimal conditions for that line, and this location can vary as the continuum flux changes. An example of a grid of emission line strengths in an LOC photoionization equilibrium model is shown in Fig. 8.

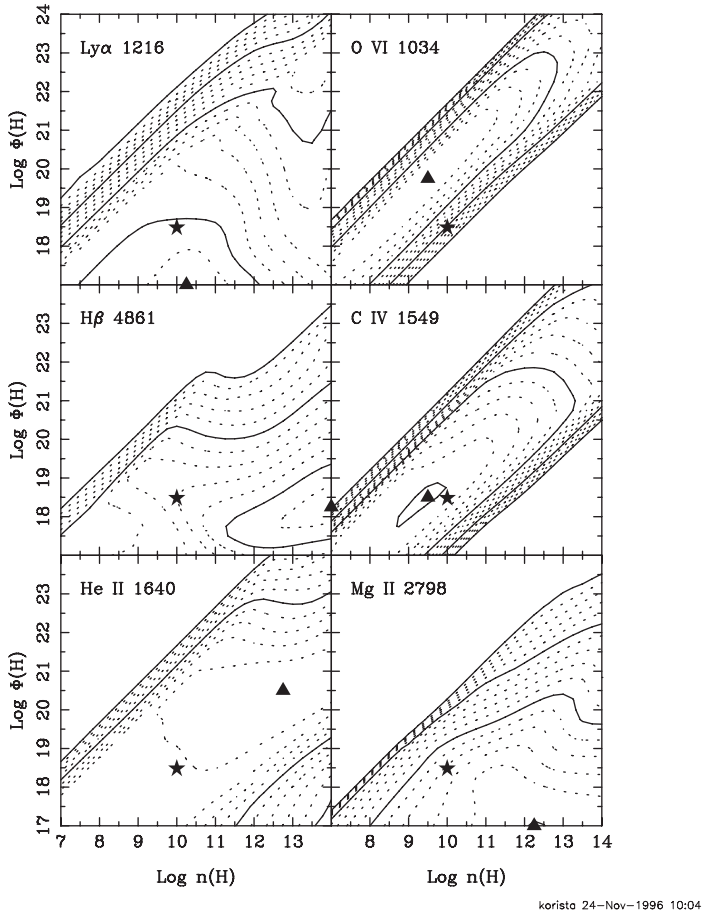


**Fig. 8.** Contours of constant equivalent width for a grid of photoionization equilibrium models, as a function of input ionizing flux ($\Phi(\mathrm{H}) = Q_{\mathrm{ion}}/4\pi r^2$) and particle density $n(H)$ for strong emission lines in AGN spectra. Dotted contours are separated by 0.2 dex and solid contours by 1 dex. The solid star is a reference point to "standard BLR parameters," i.e., the best single-zone model. The triangle shows the location of the peak equivalent width for each line. From [17]

### 4.2 Reverberation and AGN Black Hole Masses

As shown in Fig. 5, for AGNs with multiple reverberation measurements, there is virial relationship between line width and lag. This is strong evidence that the broad lines can be used to measure the mass of the central black hole via the virial theorem,

$$M_{\mathrm{BH}} = \frac{f c\tau \Delta V^2}{G}, \tag{7}$$

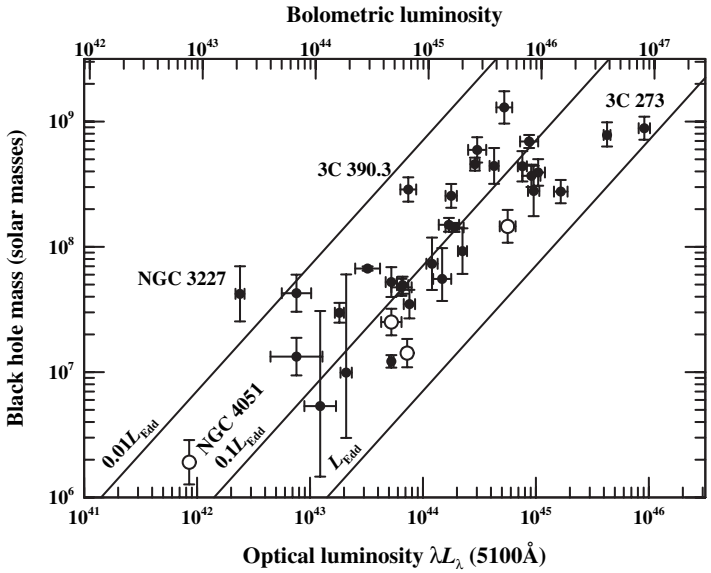


**Fig. 9.** The mass–luminosity relationship for reverberation-mapped AGNs. The luminosity scale on the lower x-axis is $\log \lambda L_\lambda$ in units of ergs $s^{-1}$. The upper x-axis shows the bolometric luminosity assuming that $L_{\rm bol} \approx 9\lambda L_\lambda(5100\,\text{Å})$. The *diagonal lines* show the Eddington limit $L_{\rm Edd}$, $0.1L_{\rm Edd}$, and $0.01L_{\rm Edd}$. The *open circles* represent NLS1s. From [25]

where $f$ is a factor of order unity that depends on the unknown geometry and kinematics of the BLR. That these virial masses are valid at some level is demonstrated by the fact that a plot of the reverberation-based masses versus the stellar bulge velocity dispersion $\sigma_*$ is consistent with the same $M_{\rm BH} - \sigma_*$ relationship seen in quiescent galaxies based on masses measured primarily by stellar or gas dynamics, e.g., [12, 13]. Indeed, a mean value for the scaling factor $f$ in (7) can be obtained by scaling the AGN $M_{\rm BH} - \sigma_*$ relationship to that for quiescent galaxies. Unfortunately, however, most dynamical models of the BLR give similar values of $f$, so this affords no useful constraint on the BLR structure and kinematics.

Figure 9 shows the relationship between black hole mass and luminosity for the 35 reverberation-mapped AGNs. All of the AGNs are sub-Eddington, contrary to some earlier estimates, and based on an admittedly nominal bolometric correction, the accretion rates are typically about 10% of the Eddington rate, but with considerable scatter about this value. The scatter in this mass-luminosity relationship is apparently real; the NLS1s occupy the right-hand edge of the envelope, as expected, and the one reverberation-mapped AGN with very broad double-peaked emission lines (see below), 3C 390.3, is on the left-hand side of the envelope, again as expected. Of course, the scatter in the relationship is not attributable only to differences in accretion rate,

but other effects such as inclination and obscuration (e.g., the luminosity of NGC 3227 is probably underestimated as it appears to have heavy internal absorption).

## 5 What is the BLR?

The fundamental question that we still have not yet addressed is what is the nature of the BLR? What is the origin of the gas that gives rise to the emission lines, and how is it related to the accretion flow, if at all? A number of different scenarios have been proposed, and we discuss some of these briefly.

### 5.1 "Cloud" Models

Our first notions of what the BLR might look like was based on observations of Galactic nebulae, especially the Crab Nebula system of "clouds" or "filaments," partly because of the obvious merits of such an interpretation (e.g., we noted earlier that supersonic motions of BLR gas argue for such a system or some kind of large-scale flow), but probably also because the first astrophysicists to work on the problem had previously worked on nebular physics in Galactic sources.

If we suppose that the BLR is comprised of some large number $N_c$ of identical line-emitting clouds of radius $R_c$, the BLR covering factor (i.e., fraction of the sky covered by BLR clouds, as seen by the central source) will be proportional to $N_c R_c^2$. The covering factor is determined by estimating the fraction of ionizing continuum photons absorbed by BLR clouds and reprocessed into emission lines, and is constrained to be of order $\sim$10% by the equivalent widths of the emission lines, notably Ly$\alpha$. An independent constraint is given by the total line luminosity, which is proportional to $N_c R_c^3$, i.e., the total volume of line-emitting material. By combining these two independent constraints on $N_c R_c^2$ and $N_c R_c^3$, we can independently solve for $N_c$ and $R_c$. For a typical Seyfert galaxy like NGC 5548, we find $N_c \approx 10^7$ and $R_c \approx 10^{13}\,\mathrm{cm}$. Furthermore, we can combine the size of the cloud with the putative particle density of $n_e \approx 10^{10}\,\mathrm{cm}^{-3}$, to get a cloud column density of $N_\mathrm{H} \approx 10^{23}\,\mathrm{cm}^{-2}$. Interestingly and ultimately coincidentally, this is the same order of magnitude as the first measurements of the column densities of "warm absorbers" detected in the X-ray spectra of AGNs, and it was natural to ascribe this absorption to BLR clouds along the line of sight to the very small X-ray continuum source. Finally, given the number, size, and density of the clouds, it is trivial to compute a mass for the entire BLR, which works out to be $\sim 1\,M_\odot$.

Early views on cloud dynamics were also influenced by observations of supernova remnants, the only other astrophysical environment in which line-emitting gas moves at velocities higher than $1000\,\mathrm{km\,s}^{-1}$. Either ballastic outflow (as in supernovae) or radiation pressure driven outflow can produce

logarithmic line profiles. A preference for outflow models was at least in some part driven by concerns that a gravitationally bound BLR seemed quite implausible. Prior to the advent of reverberation mapping, there was no way to determine the size of the BLR other than photoionization equilibrium modeling. Sizes predicted by single-zone (i.e., all lines produced in approximately the observed ratios by a single representative cloud) models were about an order of magnitude too large, thus leading to mass estimates that were far too large to be consistent with observed nuclear stellar kinematics.

The argument on the number of emission-line clouds is, however, flawed. The fact that the emission lines vary in response to continuum variations argues that the clouds are optically thick, in which case the emitting volume of a cloud is proportional to $R_c^2 R_{\rm S}$ where $R_{\rm S}$ is the depth of the ionized layer of the cloud (i.e., the Strömgren depth), rather than $R_c^3$, which removes the independent constraints on $N_c$ and $R_c$. However, there is a second argument that also argues for a large number of clouds, namely the smoothness of the emission-line profiles, as shown in Fig. 10. Here the argument is that a collection of clouds with a velocity dispersion of a few thousand $\mathrm{km\,s^{-1}}$, but each emitting lines of thermal widths of 10 $\mathrm{km\,s^{-1}}$, ought to produce a rather "grainy" composite line profile on account of statistical fluctuations in the number of clouds at different line-of-sight velocities. The lack of grainy structure at high spectral resolution and high signal-to-noise ratios argues either that the number of clouds must be very large or the BLR gas is some kind of continuous flow rather than in the form of discrete clouds. Even an extreme case, NGC 4395, the least luminous known Seyfert 1, has characteristically smooth line profiles. But the BLR in this source is expected to be so small that the number of individual clouds could not exceed a few thousand. This essentially leaves us only with models that involve some kind of supersonic flow, unless there is another significant source of microturbulence within the broad-line clouds.

Another interesting consequence of variability observations is the realization that there must be a large reservoir of gas throughout the BLR, but at any particular time we are detecting primarily the gas that is emitting most efficiently [2]. Thus the total mass of gas in the BLR is much larger than computed above. Estimates of the BLR mass run as high as $10^3$–$10^4\,M_\odot$.

### 5.2 "Bloated Stars" Model

An early suggestion for the origin of the broad emission lines was gas provided by stars in the nucleus, e.g., [1]. This solves a number of problems, such as fuel supply and cloud stability, but encounters other problems, notably that, except in the case of giant stars, which are relatively rare, the stellar surface gravity is too high to easily remove gas. Another problem is whether or not one can fit an adequate number of stars into the BLR, i.e., a variation on the "number of clouds" problem referred to above.

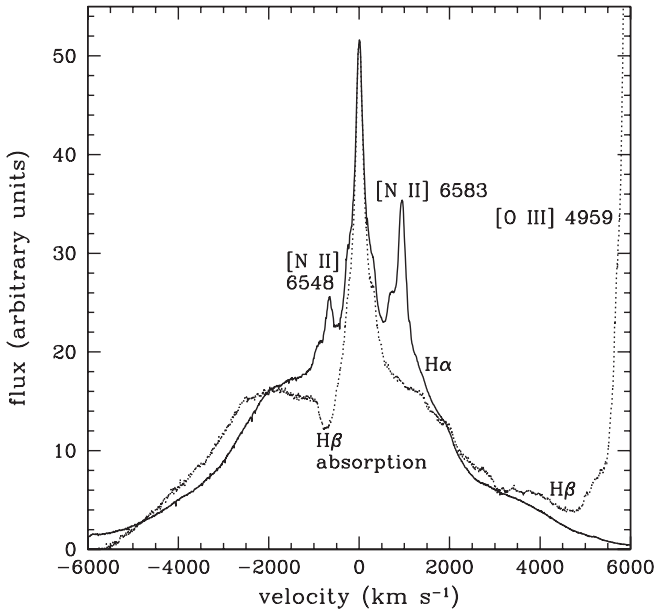


**Fig. 10.** Keck high-resolution spectra of the H$\alpha$ and H$\beta$ emission lines in NGC 4151. Some contaminating narrow-line features are labeled. While there is structure in the line profiles on scales of hundreds of km s$^{-1}$, on thermal scales the profiles are very smooth. From Arav et al., 1998, MNRAS, 297, 990

### 5.3 Double-Peaked Emission Lines

A relatively small subset of AGNs have very broad double-peaked Balmer line profiles, as shown in Fig. 11. Double-peaked profiles are characteristic of rotating disks; such profiles are commonly observed in accretion disks in Galactic binaries. Sometimes double-peaked profiles appear in the *variable* part of an AGN spectrum, i.e., the line profile that appears in difference spectra (i.e., high-state spectrum minus low-state spectrum) or in rms spectra.

Extensive efforts to model such disks indicate that they must be fairly complex. Profile variations show that the disks are clearly not axisymmetric, and they sometimes have large-scale structural or thermal irregularities. Sources with double-peaked emission lines are certainly important to our understanding of AGNs, as these are the only sources where we can identify a plausible disk structure. Whether or not such disk structures are present and merely hidden or disguised in other AGNs remains an open question. Clearly, however, disk-like structures cannot explain everything about the BLR.

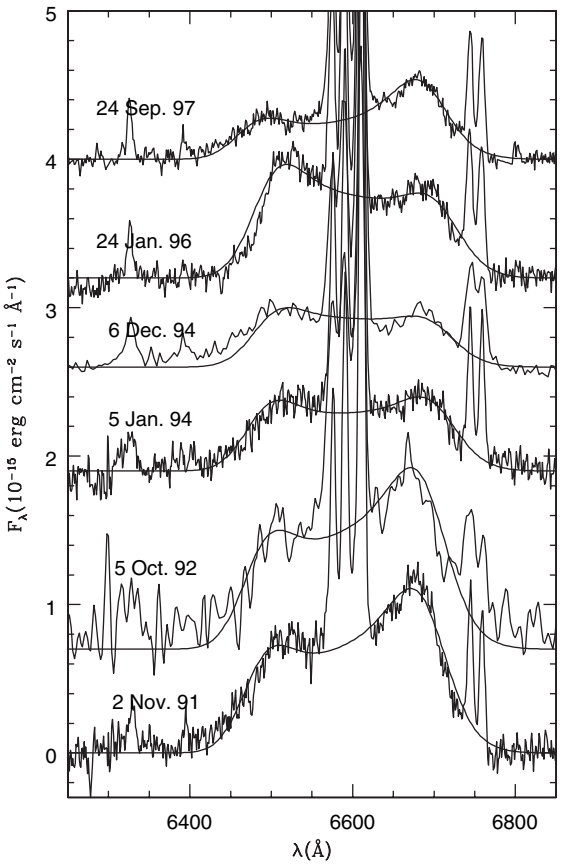


**Fig. 11.** The variable double-peaked H$\alpha$ line profile in NGC 1097, with best-fit elliptical disk models shown as solid lines. From [29]

### 5.4 Disk Winds

There is increasing evidence for the existence of disk winds in AGNs, e.g., [6, 10, 19]. Disk winds are observed in both Galactic binaries and in young stellar objects, and may be a feature common to accretion disks on all scales. There has been much theoretical investigation in this area, but it is not clear whether AGN disk winds ought to be driven radiatively or hydromagnetically, or perhaps by some hybrid.

It may well be that what we think of as the BLR is itself a composite. Photoionization equilibrium modeling has suggested that there must be two distinct regions, one highly ionized and of moderate optical depth and another of moderate ionization and greater optical depth, but of similar physical scale and distance from the central source, e.g., [8]. The latter, which is largely responsible for the Balmer-line emission, has been often identified with

the disk itself; and indeed the double-peaked Balmer lines in some sources support this. The higher ionization lines, however, may represent a disk wind component. Observational evidence for this includes:

1. clear blueward asymmetries in the higher-ionization lines in narrow-line Seyfert 1 galaxies, e.g., [18];
2. the peaks of high ionization lines tend to be blueshifted relative to systemic, and the maximum observed blueshift increases with source luminosity, e.g., [11];
3. in radio-loud quasars, the width of the bases of the C IV lines are larger in edge-on sources than in face-on sources, implying that the wind has a strong radial component to it, e.g., [30].

The disk wind model also affords a possible connection to the outflows detected in AGNs of all luminosity. Strong absorption features, generally blueshifted relative the systemic velocities, are ubiquitous features of the X-ray and UV spectra of AGNs, e.g., [9]. In high-luminosity quasars, the outflows are manifest as "broad absorption-line (BAL)" quasars. In lower-luminosity Seyfert galaxies, the features are weaker, but may still cover a fairly large velocity range, but with multiple discrete components as opposed to more-or-less continuous absorption troughs as in BAL quasars. In Seyfert galaxies, the amount of kinetic energy in the absorbing region can easily be of the same order as the radiative energy; in any given case, this calculation is subject to uncertainties due to unknown covering factors, which are quite reasonably assumed to be high because strong absorption features are so common in these sources.

## 6 What will it Take to Map the Broad-Line Region?

The BLR has been studied extensively for over 30 years. Despite this long history, new surprises seem to emerge regularly. An important recent step has been the Sloan Digital Sky Survey, which is providing extremely large samples of AGNs for statistical study.

Probably the most obvious area of untapped potential remains reverberation mapping. Emission-line response times have been measured for only 35 AGNs; the response of the high-ionization UV lines has been measured in only in a bare handful of these cases, and only in the case of NGC 5548 have measurements been made on multiple occasions.

Most importantly, however, is that *no reliable velocity-delay map has been obtained for any source.* There have been attempts to recover velocity-delay maps from reverberation data, but in every case to date, the data have been of insufficient quality or quantity for this analysis. However, as a result of these pioneering observational studies, we understand the characteristics of AGN continuum and emission-line variability well enough that we can carry out fairly realistic simulations to determine what kind of data are necessary

to recover a velocity-delay map. Extensive numerical simulations, e.g., [15], have shown the typical data requirements for a bright Seyfert galaxy (with specific numbers appropriate for the case of NGC 5548) are:

1. *High time resolution* ($\Delta t \approx 0.2$–$1.0$ day). The time sampling of the light curves translates directly into the time resolution of the velocity-delay maps. Sampling as crude as $\sim$1 day provides around 4–20 resolution elements through the line response for a typical Seyfert galaxy, depending on the particular emission-line and on the luminosity of the source.
2. *Long duration* (several months). A rule of thumb in time series is that the duration of the experiment should be at least three times as long as the longest time scale phenomenon to be addressed. This suggests a minimum duration of some 60–80 days, again depending on the emission line and continuum luminosity. What simulations show is that the main requirement for detecting a clear reverberation signal is a major "event" in the driving light curve, i.e., an outburst, "drop-out," or change in the sign of the derivative. One needs to detect a strong signal and then follow it as it propagates through the entire BLR. Simulations based on the behavior of NGC 5548 suggest that a 200-day program is necessary for a high probability of success, but success can occur with programs as short as 75 days or so, if one is lucky.
3. *Moderate spectral resolution* ($\sim$600 km s$^{-1}$). Spectral resolution translates directly into velocity-resolution in the velocity-delay map. Resolution of $R > 500$ typical yields some 10 or so resolution elements across a typical broad emission line. Given the lack of profile structure at high spectral resolution, resolution approaching the thermal line width (i.e., $R \approx 30,000$) does not seem necessary.
4. *High homogeneity and signal-to-noise ratio ($S/N \approx 100$).* A high level of homogeneity and high signal-to-noise ratios per datum are required in order to detect the continuum variations, usually a few percent or less between observations, and the responding signal in the emission lines. At least high *relative* photometric accuracy is required; this is a major challenge to ground-based observations where one has little control over the point-spread function, which ultimately limits the photometric accuracy. For this reason and that some of the most responsive emission line are in the UV, space-based observations are preferred for obtaining velocity-delay maps.

Detailed simulations show that *Hubble Space Telescope* can carry out such a project, but practically speaking, only for a limited number of emission lines. To get a complete map of the BLR, it is desirable to use as many lines as possible; this is especially important if the BLR is, as suggested earlier, a composite structure such as a disk plus a disk wind. A space mission concept, called *Kronos*, has been designed to obtain spectroscopic time series data on accretion-driven sources, with the specific application of obtaining velocity-delay maps of the BLR as a major goal. The key to *Kronos* science is long

on-target times at high time resolution, enabled by long on-target times as a consequence of its high-Earth orbit ($P \approx 14$ days).

Figure 12 shows an example of a reverberation-mapping simulation. The BLR model in this case is an inclined ($i = 45°$) Keplerian disk with a somewhat arbitrary spiral-arm structure. The emission-line response for each of four strong lines is calculated from a photoionization equilibrium model based on NGC 5548. The recovered velocity-delay maps are based on the quality and quantity of data expected from the *Kronos* spectrometers.

## 7 Some Obvious Questions to Keep in Mind

Any explanation for the origin of the BLR must provide answers to a number of fairly obvious questions:

1. Stellar-mass black hole systems (microquasars) do not have (obvious) BLRs. Why are they different from AGNs? While Galactic binaries have accretion disks and jets, they do not have anything like the BLR. This may, of course, be related to the fact that accretion disks around stellar-mass black holes are considerably hotter than those around supermassive black holes, as the highest disk temperature is inversely proportional to the mass in simple thin-disk models.
2. Some AGNs may lack BLRs, i.e., they are true type 2 AGNs. Whereas many type 2 AGNs have "hidden" BLRs that are detected at extremely high signal-to-noise ratios or in polarized (scattered) light, there is evidence suggesting that some Type 2 objects have no broad lines at all. Why is this? What are the physical differences between AGNs with BLRs and those without?
3. Broad lines widths are in the range 1000 to 25,000 $\mathrm{km\,s^{-1}}$. What imposes these limits? And, a key question closely related to this, what does spectrum of an AGN at $i = 0°$ look like? If not orbital motion, what causes the line broadening in this extreme case?
4. Where does the energy to power the emission lines come from? The BLR energy budget problem is still unsolved. The observed AGN continuum is neither luminous enough nor hard enough to account for the broad lines. Does the BLR see a different continuum than we do, or is there an energy source we have not yet recognized?

## 8 Summary

Despite years of observational and theoretical effort, we cannot yet say much about the BLR with any certainty. We know that it is dense by nebular standards and hot ($T \approx 10^4$ K), and that it is probably some supersonic, fairly continuous flow. The dynamics of the BLR are unknown, though it

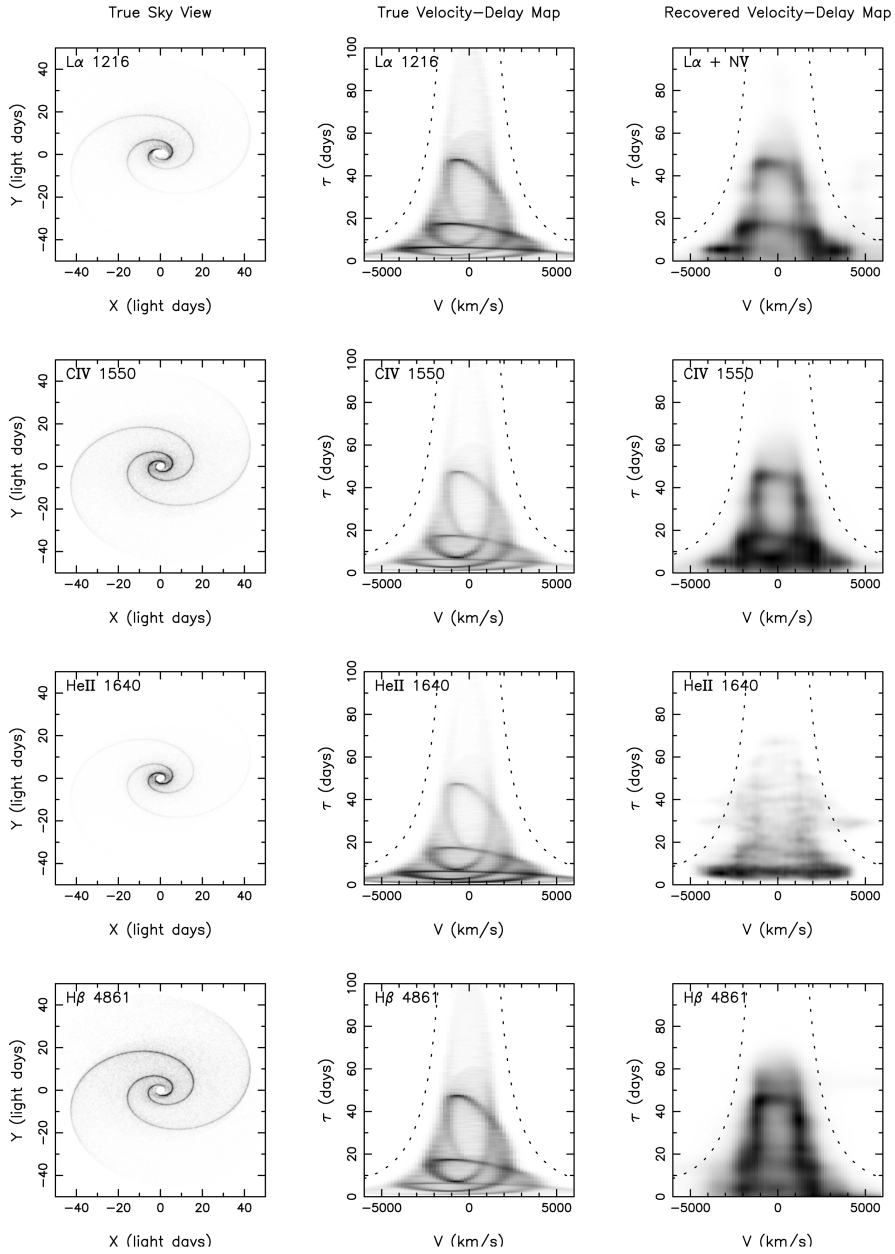


**Fig. 12.** Reverberation mapping simulations. From left to right, the three columns show, for four emission lines, (**a**) a map of a BLR with a spiral arm structure in configuration space, (**b**) a corresponding velocity-delay map, and (**c**) a velocity-delay map recovered from simulated data. From top to bottom, the rows represent results for Ly$\alpha$ $\lambda$1216, C IV $\lambda$1550, He II $\lambda$1640, and H$\beta$ $\lambda$4861. From [15]

is clear that the gravitational acceleration caused by the central source is sufficiently dominant that we can use the BLR size and velocity dispersion to estimate the central black hole masses with an accuracy of about a factor of three. We know that it has a stratified ionization structure, and may have multiple kinematic components; currently strong candidates include both disk winds and emission from the extended parts of the accretion disk itself, with the strength of different components varying from object to object and from emission line to emission line. We know that the size of the BLR scales simply with luminosity, both globally from object-to-object and in a single source as the mean luminosity varies with time. The latter in particular argues that there is considerably more mass involved in the BLR than presumed by naive models. We have argued that the best way to determine the structure and kinematics of the BLR is by obtaining velocity-delay maps for multiple emission lines by reverberation mapping, and that the data requirements, while somewhat daunting, are realizable with existing technology.

## Acknowledgements

I am grateful for support of this work by the US National Science Foundation through grant AST-0205964 to The Ohio State University. I would like to thank my collaborators and Nahum Arav, Kirk Korista, Thaisa Storchi-Bergmann, and Dan Vanden Berk for assistance with figures. I also thank the organizers for their fine hospitality in Chile. I apologize for the incomplete nature of the reference list; the few selected references are intended to provide the reader an entry point to the extensive literature on the broad-line region rather than a comprehensive bibliography.

## References

1. T. Alexander, H. Netzer: MNRAS, **284**, 967 (1997)
2. J.A. Baldwin, G. Ferland, K.T. Korista, F. Hamann, M. Dietrich: ApJ, **582**, 590 (2003)
3. J.A. Baldwin, G. Ferland, K.T. Korista, D. Verner: ApJL, **455**, L119 (1995)
4. R.D. Blandford, C.F. McKee: ApJ, **255**, 419 (1982)
5. T.A. Boroson, R.F. Green: ApJS, **80**, 109 (1992)
6. M. Bottorff, K.T. Korista, I. Shlosman, R.D. Blandford: ApJ, **479**, 200 (1997)
7. S. Collier et al.: ApJ, **500**, 162 (1998)
8. S. Collin-Souffrin, M. Joly, D. Pequignot, S. Dumont: A&A, 166, 27 (1986)
9. D.M. Crenshaw, S.B. Kraemer, I.M. George: ARAA, **41**, 117 (2003)
10. M. Elvis: ApJ, **545**, 63 (2000)
11. B. Espey: Velocity Diagnostics of the Broad Emission-Line Region of Active Galactic Nuclei. In: *Emission Lines in Active Galaxies: New Methods and Techniques*, ed. by B.M. Peterson, F.-Z. Cheng, A.S. Wilson (Astronomical Society of the Pacific 1997) pp 175–178

12. L. Ferrarese, R.W. Pogge, B.M. Peterson, D. Merritt, A. Wandel, C.L. Joseph: ApJ, **555**, L79 (2001)
13. K. Gebhardt et al.: ApJ, **543**, L5 (2000)
14. F. Hamann, G.J. Ferland: ARAA, **37**, 487 (1999)
15. K. Horne, B.M. Peterson, S. Collier, H. Netzer: PASP, **116**, 465 (2004)
16. S. Kaspi, P.S. Smith, H. Netzer, D. Maoz, B.T. Jannuzi, U. Giveon: ApJ, **533**, 631 (2000)
17. K.T. Korista, J.A. Baldwin, G. Ferland, D. Verner: ApJS, **108**, 401 (1997)
18. K.M. Leighly: *ASCA* (and *HST*) Observations of NLS1s. In:*New Astronomy Reviews*, ed. by Th. Boller, W.N. Brandt, K.M. Leighly, M.J. Ward (Elsevier: Amsterdam 2000) pp 395–402
19. N. Murray, J. Chiang: ApJ, **474**, 91
20. H. Netzer: AGN Emission Lines. In:*Active Galactic Nuclei*, ed. by T.J.-L. Courvoisier, M. Mayor (Springer-Verlag, Berlin Heidelberg New York 1990) pp 57–160
21. H. Netzer: Physical Processes in Starburst and Active Galaxies. In: *The Starburst–AGN Connection*, ed. by I. Aretxaga, D. Kunth, R. Mújica (World Scientific: Singapore 2001) pp 117–165
22. B.M. Peterson: PASP, **105**, 247 (1993)
23. B.M. Peterson, *An Introduction to Active Galactic Nuclei*, (Cambridge University Press: Cambridge 1997)
24. B.M. Peterson: Variability of Active Galactic Nuclei. In:*The Starburst–AGN Connection*, ed. by I. Aretxaga, D. Kunth, R. Mújica (World Scientific: Singapore 2001) pp 3–67
25. B.M. Peterson, L. Ferrarese, K.M. Gilbert, S. Kaspi, M.A. Malkan, D. Maoz, D. Merritt, H. Netzer, C.A. Onken, R.W. Pogge, M. Vestergaard, A. Wandel: ApJ, **613**, 682 (2004)
26. B.M. Peterson, A. Wandel: ApJL, **521**, L95 (1993)
27. B.M. Peterson et al.: ApJ., **581**, 197 (2002)
28. J.W. Sulentic, P. Marziani, D. Dultzin-Hacyan: ARAA, **38**, 521 (2000)
29. T. Storchi-Bergmann, R. Nemmen da Silva, M. Eracleous, J.P. Halpern, A.S. Wilson, A.V. Filippenko, M.T. Ruiz, R.C. Smith, N.M. Nagar: ApJ, **598**, 956 (2003)
30. M. Vestergaard, B.J. Wilkes, P.D. Barthel: ApJ, **538**, 103 (2000)